AIP | Journal of Applied Physics

Optimisation of amorphous zinc tin oxide thin film transistors by remote-plasma reactive sputtering

K. M. Niang, J. Cho, S. Heffernan, W. I. Milne, and A. J. Flewitt

Citation: Journal of Applied Physics **120**, 085312 (2016); doi: 10.1063/1.4961608
View online: http://dx.doi.org/10.1063/1.4961608
View Table of Contents: http://scitation.aip.org/content/aip/journal/jap/120/8?ver=pdfcov
Published by the AIP Publishing

Articles you may be interested in

Amorphous indium-tin-zinc oxide films deposited by magnetron sputtering with various reactive gases: Spatial distribution of thin film transistor performance
Appl. Phys. Lett. **106**, 023502 (2015); 10.1063/1.4905654

Atomic layer deposited zinc tin oxide channel for amorphous oxide thin film transistors
Appl. Phys. Lett. **101**, 113507 (2012); 10.1063/1.4752727

High-stability oxygen sensor based on amorphous zinc tin oxide thin film transistor
Appl. Phys. Lett. **100**, 262908 (2012); 10.1063/1.4731773

Zinc tin oxide thin-film transistors via reactive sputtering using a metal target
J. Vac. Sci. Technol. B **24**, L23 (2006); 10.1116/1.2345206

High mobility transparent thin-film transistors with amorphous zinc tin oxide channel layer
Appl. Phys. Lett. **86**, 013503 (2005); 10.1063/1.1843286

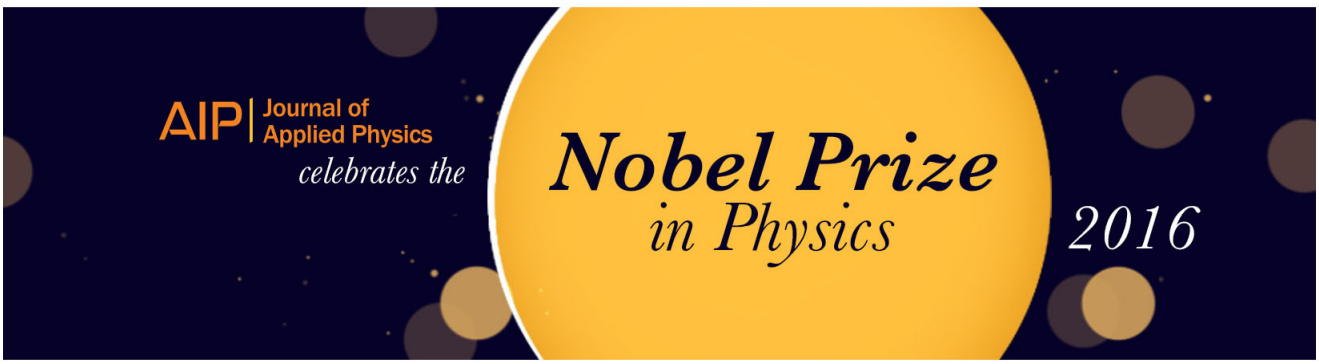

Reuse of AIP Publishing content is subject to the terms at: https://publishing.aip.org/authors/rights-and-permissions. Download to IP: 131.111.184.102 On: Thu, 20 Oct 2016 10:33:10

Optimisation of amorphous zinc tin oxide thin film transistors by remote-plasma reactive sputtering

K. M. Niang, J. Cho, S. Heffernan, W. I. Milne, and A. J. Flewitt
Electrical Engineering Division, Department of Engineering, University of Cambridge, 9 JJ Thomson Avenue, Cambridge CB3 0FA, United Kingdom

(Received 30 May 2016; accepted 12 August 2016; published online 29 August 2016)

The influence of the stoichiometry of amorphous zinc tin oxide (a-ZTO) thin films used as the semiconducting channel in thin film transistors (TFTs) is investigated. A-ZTO has been deposited using remote-plasma reactive sputtering from zinc:tin metal alloy targets with 10%, 33%, and 50% Sn at. %. Optimisations of thin films are performed by varying the oxygen flow, which is used as the reactive gas. The structural, optical, and electrical properties are investigated for the optimised films, which, after a post-deposition annealing at 500 °C in air, are also incorporated as the channel layer in TFTs. The optical band gap of a-ZTO films slightly increases from 3.5 to 3.8 eV with increasing tin content, with an average transmission ~90% in the visible range. The surface roughness and crystallographic properties of the films are very similar before and after annealing. An a-ZTO TFT produced from the 10% Sn target shows a threshold voltage of 8 V, a switching ratio of 10^8, a sub-threshold slope of 0.55 V dec^{-1}, and a field effect mobility of 15 cm^2 V^{-1} s^{-1}, which is a sharp increase from 0.8 cm^2 V^{-1} s^{-1} obtained in a reference ZnO TFT. For TFTs produced from the 33% Sn target, the mobility is further increased to 21 cm^2 V^{-1} s^{-1}, but the sub-threshold slope is slightly deteriorated to 0.65 V dec^{-1}. For TFTs produced from the 50% Sn target, the devices can no longer be switched off (i.e., there is no channel depletion). The effect of tin content on the TFT electrical performance is explained in the light of preferential sputtering encountered in reactive sputtering, which resulted in films sputtered from 10% and 33% Sn to be stoichiometrically close to the common Zn_2SnO_4 and $ZnSnO_3$ phases. © *2016 Author(s). All article content, except where otherwise noted, is licensed under a Creative Commons Attribution (CC BY) license (http://creativecommons.org/licenses/by/4.0/).*
[http://dx.doi.org/10.1063/1.4961608]

I. INTRODUCTION

For over two decades, hydrogenated amorphous silicon (a-Si:H) has dominated as the material of choice for the channel semiconductor in thin film transistors (TFTs) for display backplanes.[1] Recently, amorphous oxide semiconductors (AOSs) have been identified as a promising alternative to a-Si:H, due to their higher field effect mobility, high transparency, scalability to large substrate areas, and possibility of processing at low temperatures, making them very attractive for display backplanes and future flexible electronics.[2] While the quaternary oxide semiconductors such as indium-gallium-zinc oxide (IGZO) have been leading the way in oxide TFTs,[3,4] a simpler ternary compound, such as Zinc Tin Oxide (ZTO), is very favourable from an economic point of view as this material system does not contain expensive and/or resource-scarce elements like indium and gallium.[5]

Early investigations of ZTO focussed on its use as transparent conducting oxides (TCOs).[6–11] ZTO thin films produced by rf magnetron sputtering have a wide band gap (~3.6 eV), are n-type semiconductors with dominant crystal structures of $ZnSnO_3$ or Zn_2SnO_4, and show electrical resistivity ~4×10^{-3} and ~10^{-3} Ω cm, respectively.[6,8] While these values are respectable, they cannot compare with the leading TCO materials such as tin-doped indium oxide (ITO),[12] which is attributed to the difficulty in producing single crystalline oxides[10] and localised disorder of tin in the polycrystalline ZTO.[11] Despite these challenges, highly conductive and transparent ZTO TCOs have recently been demonstrated for large-area flexible organic light emitting diodes (OLEDs).[13] Moreover, ZTO is highly resistant to atmospheric influences and chemical treatments; as such this property has been exploited in other applications such as the active material in gas sensors,[14] the buffer layer in solar cells,[15,16] and passivation layers in IGZO TFTs.[17]

With the emergence of ionic oxides as channel materials in TFTs,[3,18,19] ZTO has also been explored previously. Chiang *et al.* first reported high performance amorphous (a-) ZTO TFTs produced by rf magnetron sputtering and with a post-deposition annealing at either 300 or 600 °C, these showed a mobility up to 50 cm^2 V^{-1} s^{-1}, with a drain current switching ratio >10^7.[20] In addition, Gorrn *et al.* have investigated the stability of a-ZTO TFTs under gate bias stress and showed a small threshold voltage shift of 30 mV after 1000 min stressing,[21] thereby demonstrating that ZTO TFTs are suitable as current drivers for transparent active matrix OLED displays.[22]

Various deposition techniques, such as sol-gel,[23,24] atomic layer deposition (ALD),[25,26] metal organic chemical vapour deposition (MOCVD),[27] and pulsed laser deposition (PLD),[21,28] have been reported for ZTO, however, rf or dc magnetron sputtering is most commonly used.[6–10,20,29–32] Ceramic ZTO targets with at. % of Zn: Sn of either 1:1 or

 © Author(s) 2016.

Reuse of AIP Publishing content is subject to the terms at: https://publishing.aip.org/authors/rights-and-permissions. Download to IP: 131.111.184.102 On: Thu, 20 Oct 2016 10:33:10

2:1 have been widely used to develop stoichiometric $ZnSnO_3$ or Zn_2SnO_4 thin films.[6–8] Separate ZnO and SnO_2 targets in combinational sputtering have also been reported to produce films with other stoichiometries.[10,31,32] The deposition rate from ceramic targets is low (a few nm min^{-1}). Ceramic targets are also expensive, and the synthesis of such targets with the required stoichiometry is no trivial matter. On the other hand, reactive sputtering techniques do not require such expensive targets since pure metal or metal alloy targets can be used. Sputtering from a metal target also means that the deposition rate is significantly higher, which is desirable for mass production. However, there are very few existing reports on the development of oxide semiconductors by reactive sputtering.[29] In this work, we explore the use of a remote reactive High Target Utilisation Sputtering (HiTUS) for the deposition of ZTO channel layers for TFTs.[33]

In the HiTUS system, a high density plasma ($\sim 10^{13}$ cm^{-3}) is generated in a side chamber by an rf electric field at 13.56 MHz and is brought onto the target in the main chamber by steering electromagnets. Applying a negative dc bias to the target increases the ion energy and initiates sputtering. The high rf launch power (maximum 2.5 kW) and target bias (maximum −1000 V) enable a wide range of sputtering conditions, thus providing a large process window. Moreover, the separation of the substrate from the plasma reduces damage from ion and electron bombardment which is typically encountered in rf magnetron sputtering.[34] These advantages have been demonstrated previously in producing high quality dielectric films such as amorphous hafnium oxide (dielectric constant ∼ 30).[35] Moreover, HiTUS has been previously employed for depositions of ZnO and InZnO for TFT applications,[36] and here is extended to a-ZTO TFTs. Films have been deposited on to various substrates from zinc:tin metal alloy targets with tin compositions of 10%, 33%, and 50% at. %. In particular, compositions of 33% and 50% are chosen to match the stoichiometry of Zn_2SnO_4 and $ZnSnO_3$. For reference, polycrystalline ZnO thin films have also been deposited by HiTUS sputtering from pure zinc metal target, using the same deposition conditions. The structural, chemical, and optical properties of the films are presented, followed by the electrical characteristics of the TFTs produced. The effect of tin content on the TFT electrical performance is explained in the light of preferential sputtering encountered in reactive sputtering.

II. EXPERIMENTAL DETAILS

ZTO and ZnO thin films were deposited onto various substrates from 100 mm diameter, zinc:tin metal alloy targets (99.99% purity) and a metallic zinc (99.999% purity) target, respectively. Typically, the chamber is evacuated to a base pressure of 2×10^{-6} mbar, while a sputtering pressure of $6–7 \times 10^{-3}$ mbar is used during coating. Argon is used for the plasma generation, and oxygen is used as the reactive gas. Before substrate coating, target cleaning was performed in argon plasma to remove any oxide formed on the surface of the target. All depositions were performed at room temperature, and the substrate temperature increased to only ∼30 °C during depositions. All films were deposited with a rf launch power/target power of 800 W/500 W and varying O_2 flow between 15 and 45 sccm (where sccm stands for standard cubic centimetres per minute. The deposition time is 12 min unless otherwise stated.

For structural characterisations, film thicknesses in the range of 200 nm–500 nm were deposited onto n-type Si (100) wafers (resistivity $\rho = 0.015–0.025\ \Omega$ cm). The film thickness was determined using a Gaertner He–Ne (633 nm) ellipsometer and Veeco Dektak profilometer. The crystallinity of the films was determined by a Phillips PW 1820 X-ray diffractometer (XRD) using a Cu-K_α radiation and a monochromator with divergence slit and receiving slit settings of 0.5 mm and 0.2 mm. The surface roughness of the films was examined using an Agilent 5400 atomic force microscope. Chemical compositions in the thin films were estimated by a Leo Gemini 1530VP FEG SEM/EDX system and a ThermoScientific Multilab-2000 X-ray photoelectron spectroscopy. The optical transmission spectrum of thin films grown on Corning 7059 glass substrates was measured using an ATI Unicam UV/Vis Spectrometer with a wavelength spectrum of 190–1100 nm. The resistivity of the films was determined at ambient temperature using an MMR Technologies Hall Effect Measurement System on films deposited on 0.8 cm × 0.8 cm glass substrates with gold top contacts, using van-der Pauw structures.

Bottom gate, inverted staggered structure TFTs were fabricated using thermally grown SiO_2 films (thickness ∼ 200 nm) on heavily doped p-type Si (100) substrates ($\rho = 0.01–0.02\ \Omega$ cm), which are used as the gate dielectric and gate electrode, respectively. Prior to channel layer depositions, the substrates were ultrasonically cleaned in acetone, isopropyl alcohol, and de-ionized water for 5 min each and then dried with N_2 followed by heating at 150 °C on a hot plate, for 5 min. The thickness of the ZTO channel layer was ∼50 nm. Some of the ZTO and ZnO films were annealed at 500 °C in an oven in air for an hour. Thermally evaporated aluminium with thickness ∼270 nm was used as the source and drain contacts. The active layer and the source/drain contacts were patterned using conventional photolithography and lift off methods. The TFTs with a channel length of 20 μm and a channel width of 1000 μm (W/L = 50) were measured in the dark, at room temperature using a Wentworth probe station inside a Faraday cage with an HP4140B dual voltage source picoammeter.

III. RESULTS AND DISCUSSION

A. Growth rate and Hall resistivity

Figure 1 shows the growth rate and Hall resistivity of the as-deposited thin films of ZTO and ZnO as a function of O_2 flow. For the ZnO films grown at an O_2 flow of 15 sccm, a growth rate of ∼50 nm min^{-1} and Hall resistivity of 1 Ω cm are observed. The growth rate decreases significantly as the O_2 flow increases, down to ∼12 nm min^{-1} for an O_2 flow of 35 sccm and higher. Meanwhile, the Hall resistivity increases to $\sim 10^6\ \Omega$ cm for O_2 flows between 25 and 45 sccm. A similar decrease in growth rate with the corresponding increase in Hall resistivity with O_2 flow is observed in the ZTO films and is true for all tin compositions investigated. The dependence of growth rate (and resistivity) on O_2

Reuse of AIP Publishing content is subject to the terms at: https://publishing.aip.org/authors/rights-and-permissions. Download to IP: 131.111.184.102 On: Thu, 20 Oct 2016 10:33:10

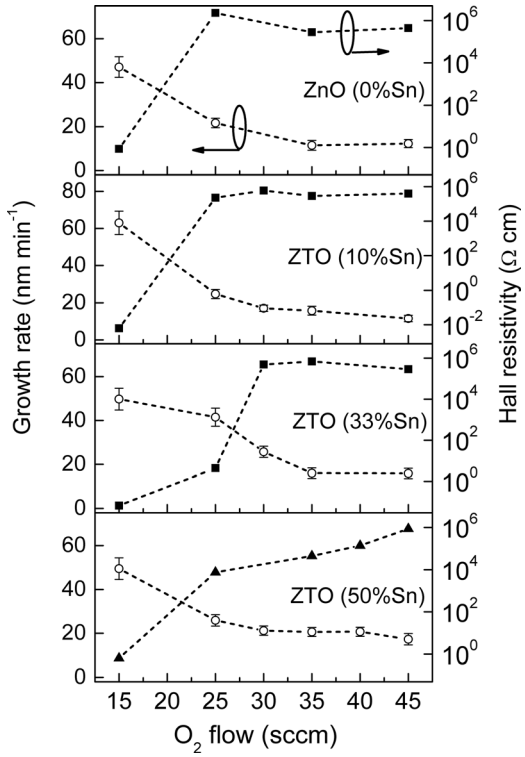

FIG. 1. Growth rate and Hall resistivity as a function of O_2 flow for the as-deposited ZnO and ZTO thin films. The Sn content (at. %) of the target used in each case is shown.

flow can be explained as follows. At a low O_2 flow, there is insufficient oxygen to react with the flux of sputtered metal species to form stoichiometric oxides. As a result, the growth rate is very high and the films are highly metallic and conductive. On the other hand, when the O_2 flow is increased, there are more O species available for the formation of metal oxides. Given that oxidation will likely take place also on the surface of the metal target (target poisoning), the sputtering current reduces resulting in a decrease in the growth rate. The films formed under this condition are transparent, highly resistive and are considered suitable for channel layers in TFTs. Such conditions are satisfied for the O_2 flow between 30 and 45 sccm, indicating a wide process window. The growth rate in this window is ~12–20 nm min^{-1}; this is much higher than that in magnetron sputtering which is typically a few nm min^{-1}.

Attempts to determine Hall mobility and carrier concentration of these highly resistive films are not successful as they are beyond the detection range of the Hall instrument. A slightly more conductive film (resistivity ~ 4 Ω cm) of ZTO sputtered with 25 sccm O_2 from 33% Sn target shows a Hall mobility of 5.7 cm^2 V^{-1} s^{-1} which is comparable to ~8 cm^2 V^{-1} s^{-1} reported for a-ZTO[28] and a-IGZO.[37] The carrier concentration of this ZTO is 2.5×10^{17} cm^{-3}; it can therefore be estimated that highly resistive films used for TFTs would have carrier concentrations $\leq 10^{17}$ cm^{-3}. On the other hand, the carrier concentrations for highly conductive films range from $\sim 5 \times 10^{19}$ to 10^{21} cm^{-3}. It should be noted that these films cannot be used straight away as TCOs, as they are opaque (see Section III B). Further process optimisation would be required to produce TCO films.[33]

B. Optical properties

Figure 2 shows the UV-visible transmission spectra of the as-deposited thin films of ZnO and ZTO as a function of O_2 flow. The thickness of each film determined either by ellipsometry or stylus profilometry is also shown. For the ZnO film deposited with 15 sccm O_2 flow, the transmittance is very low over the range of 200–700 nm. When the O_2 flow is increased to 25 sccm, there is a sudden increase in the transmittance (~90%) with the absorption edge at ~380 nm. The appearance of the film is also changed from opaque to transparent. A similar absorption edge and transmittance are observed when the O_2 flow is further increased to 35 and 45 sccm. Similar to ZnO, the ZTO films show very low transmittance with a 15 sccm O_2 flow and high transmittance (~90%) with the higher O_2 flow (25–45 sccm). Unlike ZnO, the absorption edge of the ZTO films is less abrupt and also there is a slight shift to lower wavelength as the O_2 flow increases. This trend is observed in all ZTO films with different tin compositions.

The optical band gap for the ZnO and ZTO films is determined using the Tauc relation $\alpha \cdot h\nu = B\,(h\nu - E_g)^n$, where α is the absorption coefficient, $h\nu$ is the photon energy, E_g is the band gap, B is a constant, and n is either 0.5 (for direct allowed transitions) or 2 (for indirect allowed transitions).[38] Figure 3 compares the extracted band gap of ZnO and ZTOs as a function of O_2 flow, assuming direct allowed transitions as would be expected for this material. At 35 sccm O_2 flow, the band gaps for ZnO and ZTO are 3.28 ± 0.02, 3.50 ± 0.03, 3.66 ± 0.04, and 3.81 ± 0.04 eV for the films deposited from 0%, 10%, 33%, and 50% Sn targets, respectively. For comparison, the band gaps of c-ZnO,[39] c-Zn_2SnO_4,[8,40] c-$ZnSnO_3$,[40]

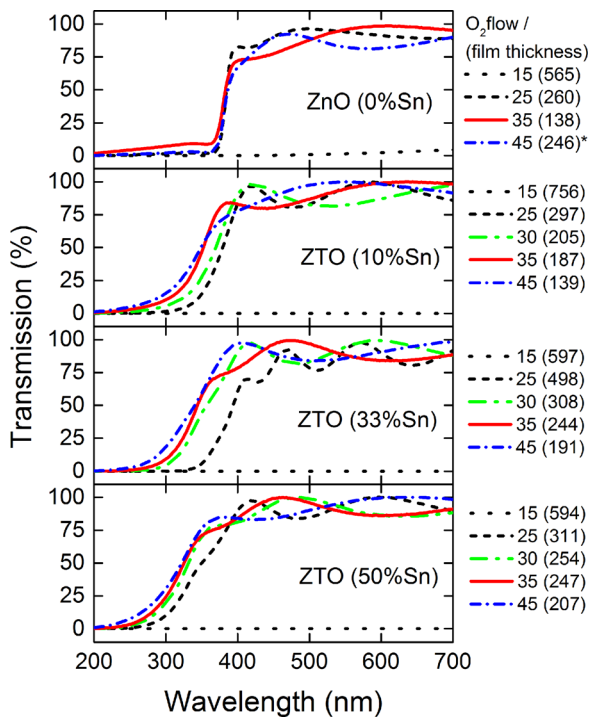

FIG. 2. Optical transmission of ZnO and ZTO as-deposited thin films deposited with various O_2 flows between 15 and 45 sccm. Value in the bracket is the film thickness measured by ellipsometry or profilometer. The deposition time is 12 min except one film marked with * which is 20 min.

Reuse of AIP Publishing content is subject to the terms at: https://publishing.aip.org/authors/rights-and-permissions. Download to IP: 131.111.184.102 On: Thu, 20 Oct 2016 10:33:10

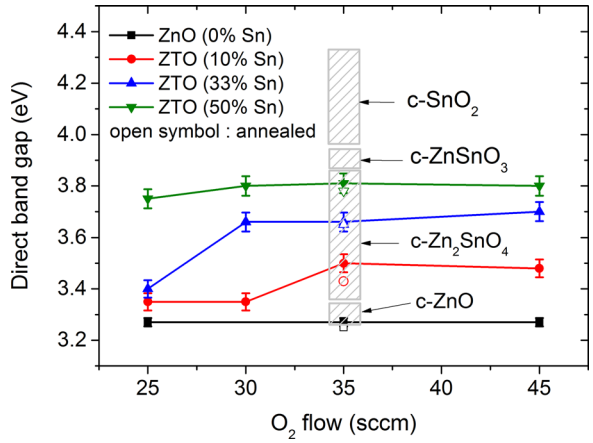

FIG. 3. Tauc band gaps of the as-deposited ZnO and ZTO as a function of tin compositions and O_2 flow. Also shown for comparison are the band gaps for c-ZnO (Ref. 39), c-Zn_2SnO_4 (Refs. 8 and 40), c-$ZnSnO_3$ (Ref. 40), and c-SnO_2 (Refs. 41 and 42). Open symbols show the Tauc band gaps of the annealed samples which are deposited with a 35 sccm O_2 flow.

and c-SnO_2[41,42] (either single-crystalline or polycrystalline) reported in the literature are also shown in Fig. 3. The ZnO band gap is very similar to the literature value. The band gaps of all our ZTOs are also comparable to the 3.35–3.89 eV range reported for polycrystalline Zn_2SnO_4 by Young *et al.*[8] Finally, also shown in Fig. 3 are the band gaps of samples which were deposited with 35 sccm O_2 flow and annealed at 500 °C in an oven in air for an hour. Only a small decrease in the band gap is observed for samples after annealing.

From Fig. 3, the effect of tin compositions on the band gap is clearly seen, showing a maximum band gap increase of ~0.53 eV between ZnO (0% Sn) and ZTO (50% Sn). Such effect can be attributed to the Burstein-Moss shift brought about by increasing carrier concentrations.[43,44] The Burstein-Moss shift due to metal cation doping has been widely reported on many TCOs such as ZTO,[8,9] aluminium-doped ZTO,[45] and aluminium-doped ZnO.[46] Moreover, a large band gap increase (up to ~1 eV) has also been reported in MOCVD ZnO, when the growth temperature is reduced from 500 to 200 °C; this was attributed to the increase in extended localization in the conduction band and valence band as the films become amorphous.[47] This situation of the film becoming amorphous is also applicable in this case, as the incorporation of Sn induces an amorphous phase in ZnO, as will be shown by XRD in Section III C. It is likely that both the Burstein-Moss shift and the amorphous phase of the film brought about by Sn incorporation contribute to the band gap increase in ZTO in this work.

It has also been reported that the oxygen partial pressure during deposition has significant effect on the band gap in TCOs.[48–50] Increase of the oxygen partial pressure is manifested in a shift of the absorption edge to longer wavelength and narrowing of the band gap (red shift). A band gap decrease ~0.18 eV is reported for ITO.[49] In our work, the band gap increase is only ~0.05 eV for the O_2 flow between 30 and 45 sccm (Fig. 3), in accordance with a small shift of absorption edge to the shorter wavelength with increasing O_2 flow (Fig. 2). The a-ZTOs produced here are aimed as AOSs for use in TFTs which means that the carrier concentrations in these films are much lower than those in TCOs. Once there is sufficient O_2 to change the deposited film from metallic to resistive (~25 sccm in this work as shown in Fig. 1), an increase of O_2 flow does not seem to have a significant effect on the band gap. Such a small change in band gap is also reported by Jayaraj *et al.* for a-ZTO prepared by PLD with O_2 partial pressures between 2 and 9 Pa.[28]

Likewise, annealing the ZTO and ZnO at 500 °C in air for 1 h only slightly decreases the optical band gap (<0.1 eV) as shown in Fig. 3. An a-ZTO film prepared by rf magnetron sputtering at 500 °C also shows a small shift of transmittance towards lower wavelength (blue shift) upon annealing at 600 °C, but a large blue shift upon annealing at 750 °C, which coincides with the appearance of crystalline peaks.[7] On the contrary, a red shift in the optical band gap (~0.5 eV) in MOCVD ZnO is reported upon annealing at 500 °C, which also coincides with an increase in the crystalline phase.[47] Since our films still remain amorphous after annealing, the small change of the optical band gap in our work is reasonable. Finally, it is also known that the thickness of the film also influences the absorption edge.[51] Since there is only a small shift the absorption edge and small change in band gap in our ZTO films, the influence of the film thickness on the band gap is considered insignificant.

C. Structural and chemical properties

The crystallographic property of the ZnO and ZTO films was checked on films deposited with an optimised O_2 flow of 35 sccm. Fig. 4 shows the θ–2θ XRD scans of the films as-deposited (a) and annealed (b) over a broad angle range ($2\theta = 20°$–$60°$). The narrow peak at 32.9° which is present for both as-deposited and annealed films corresponds to the crystalline silicon substrate as shown for reference in (c). In Fig. 4(a), the ZnO film shows a main diffraction peak at 34° which corresponds to the ZnO (002) plane, indicating the preferential *c*-axis growth of the sputtered ZnO films.[52] Fig. 4(a) also shows that the ZnO (002) peaks disappear in the as-deposited ZTO films for all tin compositions. Moreover, the

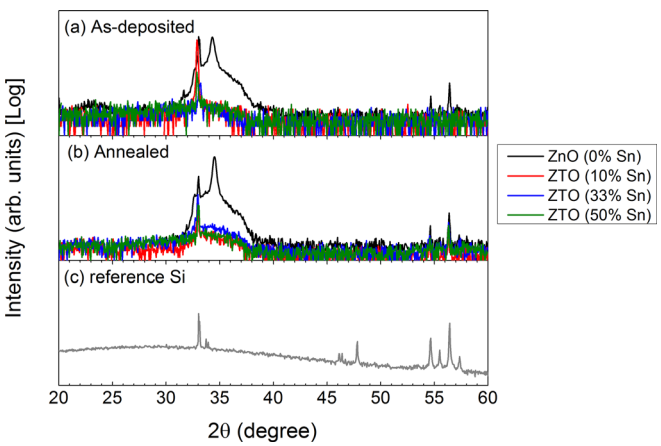

FIG. 4. X-ray diffractogram of ZnO and ZTO films as-deposited and after annealing in a θ-2θ configuration. The films are deposited with an O_2 flow of 35 sccm, and post-deposition annealing is performed at 500 °C for 1 h. Also shown is the X-ray diffractogram of a bare Si wafer for reference highlighting substrate-related peaks.

Reuse of AIP Publishing content is subject to the terms at: https://publishing.aip.org/authors/rights-and-permissions. Download to IP: 131.111.184.102 On: Thu, 20 Oct 2016 10:33:10

lack of any other distinctive diffraction peak suggests that the ZTO films are amorphous. Amorphous films are preferred over crystalline films for the production of TFTs as they yield better device-to-device uniformity over large areas.[4]

As shown in Fig. 4(b), the diffraction peak at 34° still remains in the ZnO film after annealing, indicating that the film is crystalline. This is consistent with the tendency of ZnO to remain polycrystalline. The grain size of ZnO, estimated using the Debye-Scherrer formula, is 42 nm as-deposited and 52 nm after annealing. The XRD profiles of ZTO films after annealing show that the films are still amorphous. However, a broad peak at 2θ between 31° and 38° begins to appear in ZTO films, possibly indicating the start of some medium-range ordering. At high enough temperatures, the amorphous ZTO film re-crystallizes to ZnO and SnO_2. Re-crystallization of ZTO films has been reported to start at ~600 °C in RF magnetron sputtering,[20] and <450 °C in -PLD.[28] Jayaraj *et al*. have attributed this difference to the difference in growth kinetic energies, where a higher kinetic energy in PLD produces film which recrystallizes at lower temperatures.[28] Therefore, it is reasonable to assume that in the HiTUS sputtered films, recrystallization will occur at annealing temperatures higher than 500 °C. There is no significant difference in the diffraction peaks in ZTO films despite having different tin compositions.

Figure 5 shows the AFM images of the optimised ZnO and ZTO films as-deposited (a) and after annealing at 500 °C (b). The root mean square (rms) surface roughness is compared in Figure 5(c), showing ~4 nm for ZnO and ~1.5 nm for ZTO films. Previous reported values of rms surface roughness for sputtered ZnO are ~2 nm,[52,53] which are in the same range. The values of rms surface roughness for ZTO are much smaller due to their amorphous nature and are comparable to previously reported values.[14,28] The rms surface roughness decreases slightly after annealing the a-ZTO films. The ZnO film shows similar rms surface roughness before and after annealing, but the grain size increases after annealing as clearly shown in the AFM images, agreeing with that estimated from the XRD measurements.

Finally, the chemical composition of Zn and Sn in the film is compared to that in the target for ZTO as shown in Fig. 6. XPS measurements show that the atomic composition of Sn/(Sn + Zn) is 34%, 51%, and 63% in the films deposited from the 10%, 33%, and 50% Sn targets, respectively, indicating a preferential sputtering of tin over zinc, resulting in a higher tin content in the deposited films. A lower value of tin content but a similar trend is observed from EDX measurements, also shown in Fig. 6. Compared to the target, the tin content in the film is higher by a factor of 3 for the 10% Sn target and a factor of ~1.5 for the 33% and 50% Sn targets. Higher tin content in ZTO has also been reported in films

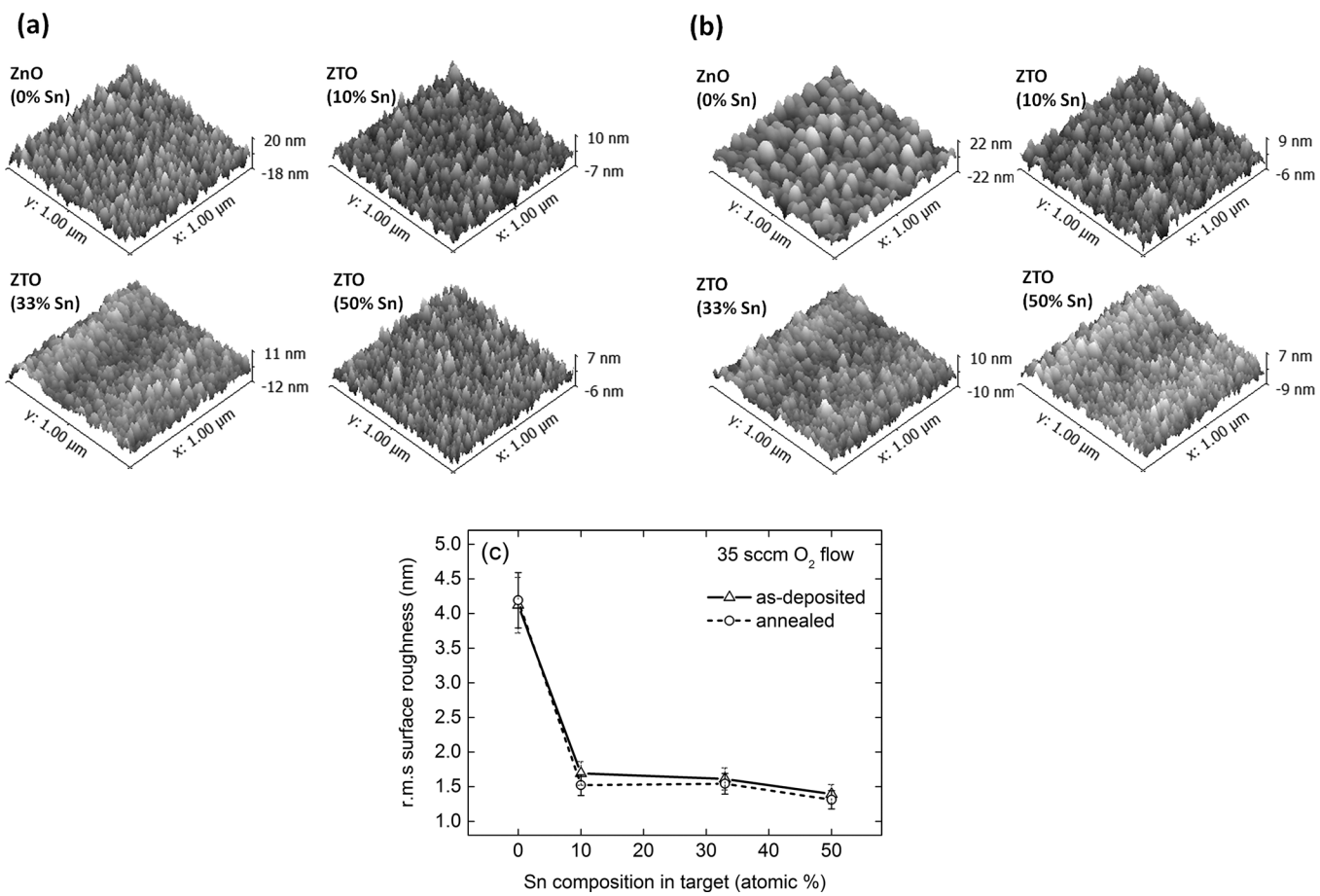

FIG. 5. (a). AFM images of ZnO and ZTO films deposited with a 35 sccm O_2 flow as-deposited and (b) after annealing at 500 °C for 1 h in air; (c) rms surface roughness of the as-deposited and annealed films as a function of atomic composition of tin in target.

Reuse of AIP Publishing content is subject to the terms at: https://publishing.aip.org/authors/rights-and-permissions. Download to IP: 131.111.184.102 On: Thu, 20 Oct 2016 10:33:10

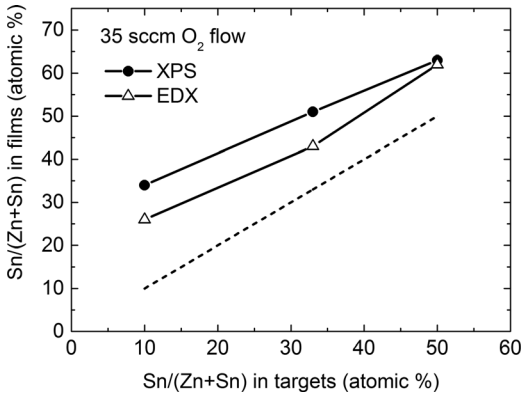

FIG. 6. Atomic composition of tin in the sputtered ZTO films as a function of that in the alloy targets for films deposited with a 35 sccm O_2 flow. Tin compositions are determined using EDX and XPS methods. The dotted line is drawn for reference which represents equal composition of tin in the target and film.

deposited by rf magnetron sputtering from ceramic targets but is less pronounced (up to a factor of 1.3).[6,7,11,54] Preferential sputtering is a common phenomenon whenever a target containing two or more elements is subjected to a particle impact, and it arises from the differences in mass, chemical binding and bombardment-induced Gibbsian segregation which are in turn related to the sputtering yield.[55] Using 500 eV Ar^+ ion as the sputtering gas, the sputtering yield of elemental tin and zinc are estimated to be 1.56 and 4.6, respectively.[56] It means that the tin content in films should have been lower than the Zn content. However, the opposite is observed in this work, which suggests that other factors are dominating the sputtering process. It can be speculated that well known phenomenon like sublimation of ZnO from the substrate might play a role.[57] Moreover, Sn-O has a higher dissociation energy than Zn-O, as shown by Mitoma *et al*. in Table I of Ref. 59, which might result in the retention of more Sn in the film than Zn.

D. Thin film transistors

The gate transfer characteristics for TFTs incorporating optimised ZnO and ZTO films both as-deposited and after post-deposition annealing are shown in Figs. 7(a) and 7(b), respectively. Following the standard field effect transistor theory,[58] the field effect mobility, μ_{FE}, and sub-threshold slope, SS, are calculated as

$$\mu_{FE} = \frac{g_m}{C_i(W/L)V_{DS}}, \tag{1}$$

where g_m is the transconductance $(\partial I_{DS}/\partial V_{GS})$, C_i is the capacitance per unit area of the gate insulator, V_{DS} is the drain source voltage, and

$$SS = \frac{dV_{GS}}{d\log(I_{DS})}, \tag{2}$$

where V_{GS} is the gate source voltage and I_{DS} is the drain source current.

Annealed ZnO TFTs operate in an accumulation mode with a threshold voltage of 18.5 V, a μ_{FE} of 0.8 $cm^2\ V^{-1}\ s^{-1}$, a switching ratio of $\sim 10^6$, and a sub-threshold slope (SS) of 2.5 V dec^{-1}. On the other hand, TFTs incorporating ZTO (10% Sn) exhibited significantly improved performance with a μ_{FE} of 14.6 $cm^2\ V^{-1}\ s^{-1}$, a threshold voltage of 8.2 V, a switching ratio of 10^8, and a sub-threshold slope of 0.55 V dec^{-1}. TFTs incorporating ZTO (33% Sn) exhibited a further increase in μ_{FE} of 21 $cm^2\ V^{-1}\ s^{-1}$ but also a slight increase in sub-threshold slope of 0.65 V dec^{-1}. The threshold voltage of ZTO (33% Sn) reduces slightly to 7.8 V. The density of the trap states, N_{it}, at the interface between ZTO and dielectric was calculated as[58]

$$N_{it} = \left(\frac{SS\log(e)}{kT/q} - 1\right)\frac{C_i}{q}, \tag{3}$$

where kT is the thermal energy and q is the electronic charge. The N_{it} of 8.2×10^{11} and 9.8×10^{11} cm^{-2} were obtained for ZTO (10% Sn) and ZTO (33% Sn), respectively.

Finally, TFTs incorporating ZTO (50% Sn) cease to function as a switch indicating that the channel cannot be depleted. Moreover, when V_{DS} is increased from 0.1 to 1 V, the drain source current, I_{DS}, is increased by two orders of magnitude. The transfer characteristics of the annealed TFTs are summarised in Table I. Interestingly, as shown in Fig. 7(a), even the un-annealed TFTs showed the effect of changing tin content. The I_{DS} varies from $\sim 10^{-12}$ A in pure ZnO, up to $\sim 10^{-6}$ A in ZTO with the highest tin content (50% Sn). ZTO TFTs with medium tin content (10% and 33%) also indicated switching behaviour.

Figure 8 shows the corresponding output characteristics of TFTs both as-deposited (a) and after post-deposition annealing (b). At applied bias $V_{GS} = 20$ V and $V_{DS} = 2$ V, the I_{DS} of annealed TFTs are 0.003, 0.23, 0.34, and 2 mA for undoped 0%, 10%, 33%, and 50% Sn, respectively, showing a trend of increasing I_{DS} with tin doping. No current crowding is observed indicating a good source drain contact to the semiconductor layer. As expected, the TFTs with as-deposited films exhibited much lower I_{DS}.

As shown in Fig. 7(b) and Table I, the μ_{FE} of ZnO TFT is only 0.8 $cm^2\ V^{-1}\ s^{-1}$. It is well known that ZnO is a the polycrystalline material and high defect density at the grain boundaries limits the performance of ZnO TFTs.[36] On the contrary, the lack of grain boundaries in the amorphous ZTO resulted in a sharp increase of the $\mu_{FE} \sim 15$ $cm^2\ V^{-1}\ s^{-1}$ in ZTO (10% Sn). In fact, obtaining an amorphous phase by incorporating one or more post transition metal cations is the basis of the multi-component amorphous oxide semiconductor system.[4] A further increase in the μ_{FE} from $\sim$15 in ZTO (10% Sn) to $\sim$21 $cm^2\ V^{-1}\ s^{-1}$ in ZTO (33% Sn) can be attributed to the effect of tin content, as more Sn ions (with valency +3 or +4) will contribute extra electrons and increase the carrier concentration. Moreover, a very low off-current ($\sim 10^{-13}$ A) is still achieved, indicating the suppression of carrier generation via oxygen vacancy formation due to high dissociation energy of the Sn-O bond.[59] This is analogous to the effect of Ga in IGZO material systems, where Ga is known as the stabilizer cation.[4,60] However, the increased mobility due to the Sn content comes at the expense of the sub-threshold slope, as observed by the increase in SS (from 0.55 to 0.65 V dec^{-1}) in the TFT sputtered from the 33% Sn target. This trade-off is magnified

Reuse of AIP Publishing content is subject to the terms at: https://publishing.aip.org/authors/rights-and-permissions. Download to IP: 131.111.184.102 On: Thu, 20 Oct 2016 10:33:10

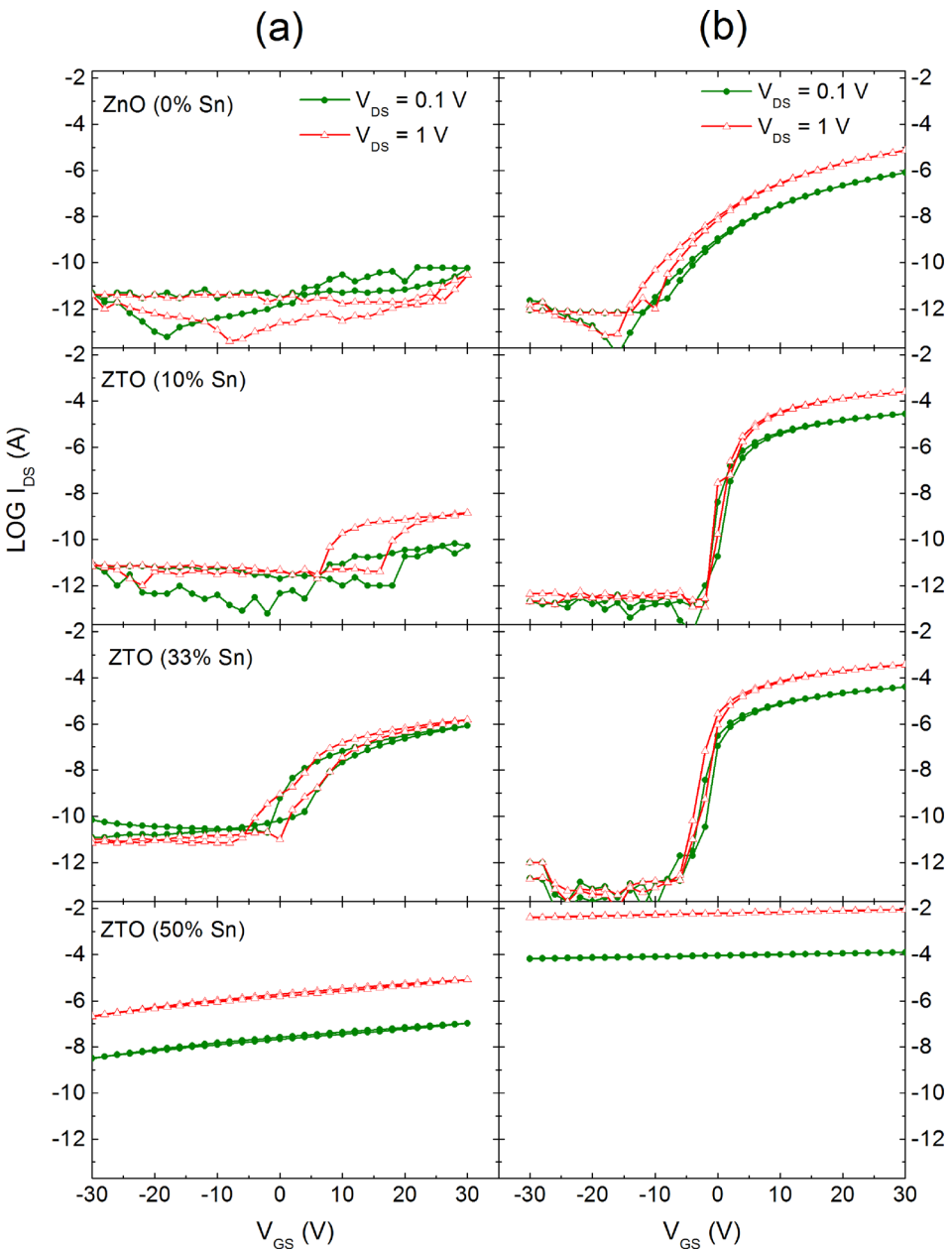

FIG. 7. Gate transfer characteristics of ZnO and ZTO TFTs with a channel *W*/*L* ratio of 50, measured with a V_{DS} of 0.1 V and 1 V. Column (a) shows devices fabricated from active layers without annealing, and column (b) shows the corresponding devices with a post-deposition annealing at 500 °C for 1 h in air.

in the ZTO TFTs sputtered from the 50% Sn target, where the sub-threshold slope can no longer be extracted and the device stops functioning as a TFT.

The density of interface trap states $\sim 9 \times 10^{11}$ cm^{-2} extracted for a-ZTO TFTs in this work are in the same range as that reported for IGZO TFTs.[61] In addition to the interface states, the defect tail states in the sub-band gap of the semiconductor (commonly expressed as Urbach energy) are known to affect TFT performance.[62] Using the photothermal deflection method, the Urbach energies of 98 and 102 meV are obtained for annealed films of ZTO (10% Sn) and ZTO (33% Sn), respectively.[63] These values are also very similar to previously reported Urbach energies ~110 meV for ZTO[64] and ~110–160 meV for IGZO.[60] The slightly lower Urbach energy of ZTO (10% Sn) comparing to ZTO (33% Sn) agrees with a slight reduction in SS of ZTO (10% Sn) comparing to ZTO (33% Sn).

TABLE I. Transistor parameters of ZnO and ZTO TFTs deposited with a 35 sccm O_2 flow with a channel *W*/*L* ratio of 50, measured with a V_{DS} of 0.1 V (as shown in Fig. 7(b)). A post-deposition annealing at 500 °C for 1 h in air is used.

	V_{th} (V)	μ_{FE} (cm^2 V^{-1} s^{-1})	SS (V dec^{-1})	I_{ON}/I_{OFF}
ZnO (0% Sn)	18.5	0.8	2.5	10^6
ZTO (10% Sn)	8.2	14.6	0.55	10^8
ZTO (33% Sn)	7.8	21.0	0.65	10^8

As shown in Fig. 6, ZTO films sputtered from 10% and 33% Sn actually include increased tin composition in the films of 34% and 51%, respectively. Interestingly, these zinc/tin compositions are very close to stoichiometric Zn_2SnO_4 and $ZnSnO_3$, respectively. This is consistent with previously reported ZTO TFTs with an atomic ratio of zinc:tin of either 2:1 or 1:1 by rf magnetron sputtering.[20,30,54]

In our work, ZTO TFTs (50% Sn) which have an actual tin content of 63% can no longer be turned off, while ZTO

Reuse of AIP Publishing content is subject to the terms at: https://publishing.aip.org/authors/rights-and-permissions. Download to IP: 131.111.184.102 On: Thu, 20 Oct 2016 10:33:10

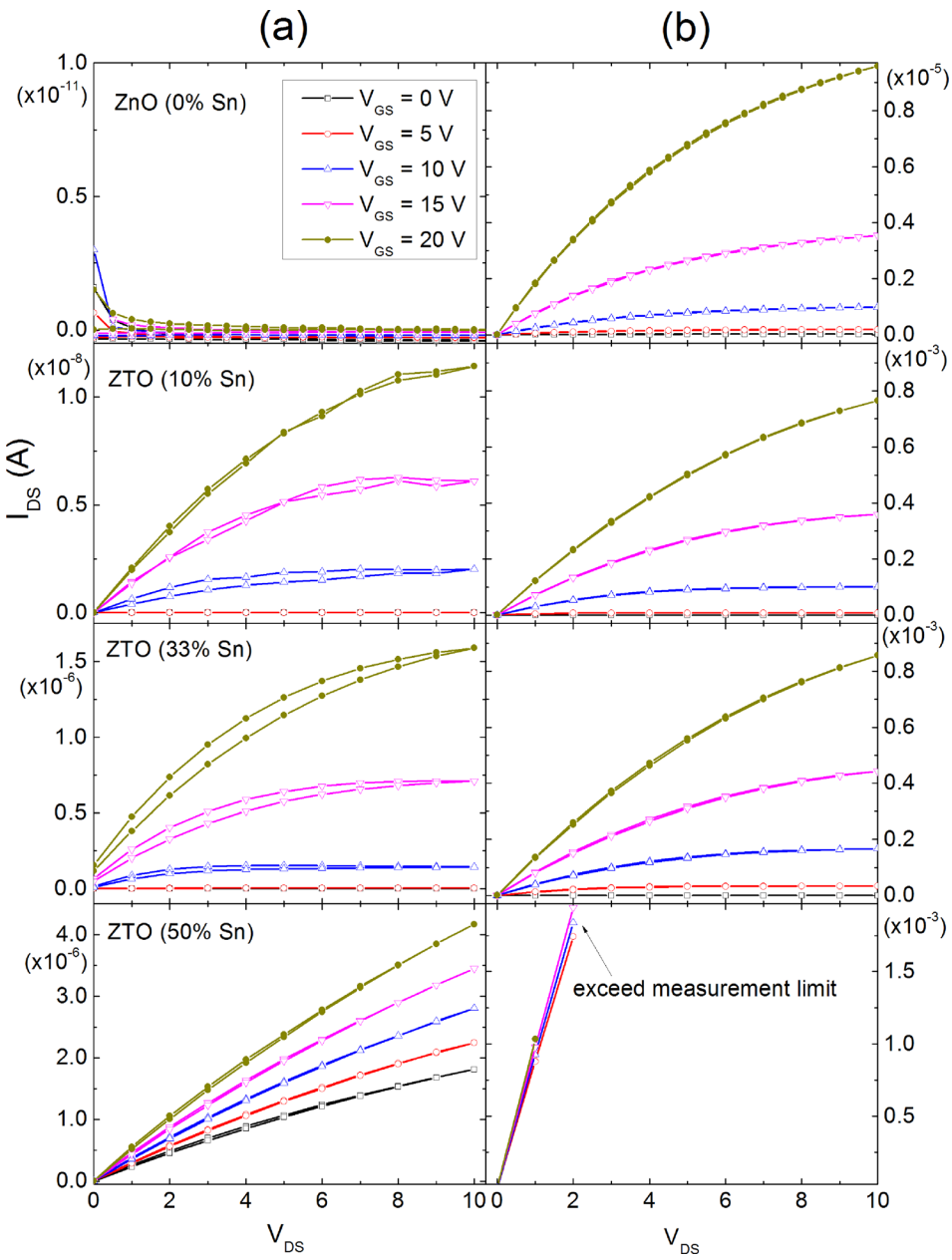

FIG. 8. Drain transfer characteristics of ZnO and ZTO TFTs with a channel *W*/*L* ratio of 50, measured with V_{GS} from 0 to 20 V in 5 V intervals. Column (a) shows devices fabricated from active layers without annealing, and column (b) shows the corresponding devices with a post-deposition annealing at 500 °C for 1 h in air.

with Sn 67% by rf sputtering still functions as a TFT with incremental mobility ~30 cm^2 V^{-1} s^{-1}.[30] Moreover, ZTO TFTs produced from combinational rf sputtering from ZnO and SnO_2 targets show a saturation mobility ~10 cm^2 V^{-1} s^{-1} and are achieved at Sn 20% and 75% content.[32] Finally, ZTO TFTs produced from MOCVD achieve field effect mobility ~7–17 cm^2 V^{-1} s^{-1} ZTO with Sn 27%, 49%, and 72% content.[27] The difference in the window of tin compositions in the ZTO in producing respectable TFTs is attributed to the different growth kinetics in each deposition technique. Despite various methodologies used, the extracted carrier mobility of TFTs produced by various deposition techniques are of the same order.

In spite of a pronounced preferential sputtering in HiTUS, optimisation of stoichiometric Zn_2SnO_4 and $ZnSnO_3$ for TFT channel could still be achieved, as shown in this work. Also shown is the high sputtering rate in HiTUS, as a channel layer deposition takes ~2–3 min only. In contrast to the use of a ceramic ZTO target in magnetron sputtering, the use of a metal alloy target in a reactive sputtering guarantees a higher deposition rate, easier manufacture of target, and thus reduced cost. Further, the use of a remote plasma and the availability of high powers in HiTUS guarantee depositions of films with high density but minimum ion bombardment from the plasma. This effect is less immediately apparent in this work, as the rf launch/ target power currently used is relatively low (800 W/500 W). Further optimisation of a-ZTO with high powers which has the potential to improve the film density and reduce post-deposition annealing temperature is under way.

IV. CONCLUSIONS

Amorphous ZTO has been produced using a remote-plasma reactive sputtering from zinc:tin metallic alloy targets with various tin compositions. The films are first

Reuse of AIP Publishing content is subject to the terms at: https://publishing.aip.org/authors/rights-and-permissions. Download to IP: 131.111.184.102 On: Thu, 20 Oct 2016 10:33:10

optimised by varying the O_2 flow, and it is observed that a large process window exists in producing highly resistive ZTO films suitable for the channel layer in TFTs. The optimised a-ZTO films displayed a larger optical band gap with increasing tin compositions. The effect of post-deposition annealing is most significant in the electrical properties of TFTs. While ZnO TFTs exhibited a poor device performance due to grain boundaries, a-ZTO TFTs exhibited a significant increase in mobility and the mobility increases with tin content up to 50 at. % of Sn in the film. Device performances are explained with the increased tin content in the films brought about by the preferential sputtering, such that films sputtered from 10% and 33% Sn targets are very close to stoichiometric $ZnSnO_3$ and Zn_2SnO_4. The difference in the sub-threshold slope between $ZnSnO_3$ and Zn_2SnO_4 is explained by the Urbach energies. In summary, a-ZTO TFTs produced by HiTUS sputtering have comparable device performances and tin composition windows to the conventional magnetron sputtering. However, HiTUS sputtering has added advantage over the conventional magnetron sputtering in its higher deposition rate and the potential to improve the density of a-ZTO films which thus lowers the annealing temperatures.

ACKNOWLEDGMENTS

The support of this work by the Engineering and Physical Sciences Research Council (EPSRC) through Project No. EP/M013650/1 was acknowledged. Additional data related to this publication are available at the DSpace@Cambridge data repository (www.repository.cam.ac.uk).

[1]A. J. Flewitt, in *Handbook of Visual Display Technology*, edited by J. Chen, W. M. Cranton, and M. Fihn (Springer, 2012), Vol. 1, p. 628.
[2]E. Fortunato, P. Barquinha, and R. Martins, Adv. Mater. **24**, 2945 (2012).
[3]K. Nomura, H. Ohta, K. Ueda, T. Kamiya, M. Hirano, and H. Hosono, Science **300**, 1269 (2003).
[4]K. Nomura, H. Ohta, A. Takagi, T. Kamiya, M. Hirano, and H. Hosono, Nature **432**, 488 (2004).
[5]C. Candelise, M. Winskel, and R. Gross, Prog. Photovoltaics: Res. Appl. **20**, 816 (2012).
[6]T. Minami, Jpn. J. Appl. Phys., Part 1 **33**, 1693 (1994).
[7]K. Satoh, Y. Kakehi, A. Okamoto, S. Murakami, F. Uratani, and T. Yotsuya, Jpn. J. Appl. Phys., Part 2 **44**, L34 (2005).
[8]D. L. Young, H. Moutinho, Y. Yan, and T. J. Coutts, J. Appl. Phys. **92**, 310 (2002).
[9]J. D. Perkins, J. A. del Cueto, J. L. Alleman, C. Warmsingh, B. M. Keyes, L. M. Gedvilas, P. A. Prarilla, B. To, D. W. Readey, and D. S. Ginley, Thin Solid Films **411**, 152 (2002).
[10]Y. Hayashi, K. Kondo, K. Murai, T. Moriga, I. Nakabayashi, H. Fukumoto, and K. Tominaga, Vacuum **74**, 607 (2004).
[11]D. L. Young, D. L. Williamson, and T. J. Coutts, J. Appl. Phys. **91**, 1464 (2002).
[12]R. B. H. Tahar, T. Ban, Y. Ohya, and Y. Takahashi, J. Appl. Phys. **83**, 2631 (1998).
[13]M. Morales-Masis, F. Dauzou, Q. Jeangros, A. Dabirian, H. Lifka, R. Gierth, M. Ruske, D. Moet, A. Hessler-Wyser, and C. Ballif, Adv. Funct. Mater. **26**, 384 (2016).
[14]S. Dutta and A. Dodabalapur, Sens. Actuators, B **143**, 50 (2009).
[15]Y. S. Lee, J. Heo, S. C. Siah, J. P. Mailoa, R. E. Brandt, S. B. Kim, R. G. Gordon, and T. Buonassisi, Energy Environ. Sci. **6**, 2112 (2013).
[16]X. Wu, S. Asher, D. H. Levi, D. E. King, Y. Yan, T. A. Gessert, and P. Sheldon, J. Appl. Phys. **89**, 4564 (2001).
[17]C. H. Kim, Y. S. Rim, and H. J. Kim, J. Phys. D: Appl. Phys. **47**, 385104 (2014).
[18]R. L. Hoffman, B. J. Norris, and J. F. Wager, Appl. Phys. Lett. **82**, 733 (2003).
[19]E. M. C. Fortunato, P. M. C. Barquinha, A. C. M. B. G. Pimentel, A. M. F. Gonçalves, A. J. S. Marques, R. F. P. Martins, and L. M. N. Pereira, Appl. Phys. Lett. **85**, 2541 (2004).
[20]H. Q. Chiang, J. F. Wager, R. L. Hoffman, J. Jeong, and D. A. Keszler, Appl. Phys. Lett. **86**, 013503 (2005).
[21]P. Görrn, P. Hölzer, T. Riedl, W. Kowalsky, J. Wang, T. Weimann, P. Hinze, and S. Kipp, Appl. Phys. Lett. **90**, 063502 (2007).
[22]P. Görrn, F. Ghaffari, T. Riedl, and W. Kowalsky, Solid-State Electron. **53**, 329 (2009).
[23]C.-G. Lee, B. Cobb, and A. Dodabalapur, Appl. Phys. Lett. **97**, 203505 (2010).
[24]S.-J. Seo, C. G. Choi, Y. H. Hwang, and B.-S. Bae, J. Phys. D: Appl. Phys. **42**, 035106 (2009).
[25]W.-S. Choi, J. Korean Phys. Soc. **57**, 1472 (2010).
[26]J. Heo, S. Bok Kim, and R. G. Gordon, Appl. Phys. Lett. **101**, 113507 (2012).
[27]U. K. Kim, S. H. Rha, J. H. Kim, Y. J. Chung, J. Jung, E. S. Hwang, J. Lee, T. J. Park, J.-H. Choi, and C. S. Hwang, J. Mater. Chem. C **1**, 6695 (2013).
[28]M. K. Jayaraj, K. J. Saji, K. Nomura, T. Kamiya, and H. Hosono, J. Vac. Sci. Technol. B **26**, 495 (2008).
[29]D. Hong, H. Q. Chiang, and J. F. Wager, J. Vac. Sci. Technol. B **24**, L23 (2006).
[30]R. L. Hoffman, Solid-State Electron. **50**, 784 (2006).
[31]J. H. Ko, I. H. Kim, D. Kim, K. S. Lee, T. S. Lee, J. H. Jeong, B. Cheong, Y. J. Baik, and W. M. Kim, Thin Solid Films **494**, 42 (2006).
[32]M. G. McDowell, R. J. Sanderson, and I. G. Hill, Appl. Phys. Lett. **92**, 013502 (2008).
[33]S. J. Wakeham, M. J. Thwaites, B. W. Holton, C. Tsakonas, W. M. Cranton, D. C. Koutsogeorgis, and R. Ranson, Thin Solid Films **518**, 1355 (2009).
[34]K. Tominaga, Y. Sueyoshi, H. Imai, M. Chong, and Y. Shintani, Jpn. J. Appl. Phys., Part 1 **32**, 4745 (1993).
[35]F. M. Li, B. C. Bayer, S. Hofmann, J. D. Dutson, S. J. Wakeham, M. J. Thwaites, W. I. Milne, and A. J. Flewitt, Appl. Phys. Lett. **98**, 252903 (2011).
[36]A. J. Flewitt, J. D. Dutson, P. Beecher, D. Paul, S. J. Wakeham, M. E. Vickers, C. Ducati, S. P. Speakman, W. I. Milne, and M. J. Thwaites, Semicond. Sci. Technol. **24**, 085002 (2009).
[37]H. Hosono, J. Non-Cryst. Solids **352**, 851 (2006).
[38]J. Tauc, R. Grigorovici, and A. Vancu, Phys. Status Solidi **15**, 627 (1966).
[39]U. Özguür, Y. I. Alivov, C. Liu, A. Teke, M. A. Reshchikov, S. Doğan, V. Avrutin, S. J. Cho, and H. Morkoç, J. Appl. Phys. **98**, 041301 (2005).
[40]M. Miyauchi, Z. Liu, Z. G. Zhao, S. Anandan, and K. Hara, Chem. Commun. **46**, 1529 (2010).
[41]G. Sanon, R. Rup, and A. Mansingh, Phys. Rev. B **44**, 5672 (1991).
[42]B. Stjerna, E. Olsson, and C. G. Granqvist, J. Appl. Phys. **76**, 3797 (1994).
[43]E. Burstein, Phys. Rev. **93**, 632 (1954).
[44]T. S. Moss, Proc. Phys. Soc. (London) B **67**, 775 (1954).
[45]K. Satoh, Y. Kakehi, A. Okamoto, S. Murakami, K. Moriwaki, and T. Yotsuya, Thin Solid Films **516**, 5814 (2008).
[46]P. Banerjee, W.-J. Lee, K.-R. Bae, S. B. Lee, and G. W. Rubloff, J. Appl. Phys. **108**, 043504 (2010).
[47]S. T. Tan, B. J. Chen, X. W. Sun, W. J. Fan, H. S. Kwok, X. H. Zhang, and S. J. Chua, J. Appl. Phys. **98**, 013505 (2005).
[48]K. Tominaga, T. Ueda, T. Ao, M. Kataoka, and I. Mori, Thin Solid Films **281**, 194 (1996).
[49]H.-N. Cui, V. Teixeira, L.-J. Meng, R. Martins, and E. Fortunato, Vacuum **82**, 1507 (2008).
[50]S. Li, X. Qiao, and J. Chen, Mater. Chem. Phys. **98**, 144 (2006).
[51]H.-M. Kim, S.-K. Jung, J.-S. Ahn, Y.-J. Kang, and K.-C. Je, Jpn. J. Appl. Phys. **42**, 223 (2003).
[52]L. García-Gancedo, J. Pedrós, Z. Zhu, A. J. Flewitt, W. I. Milne, J. K. Luo, and C. J. B. Ford, J. Appl. Phys. **112**, 014907 (2012).
[53]P. F. Carcia, R. S. McLean, M. H. Reilly, and G. Nunes, Appl. Phys. Lett. **82**, 1117 (2003).
[54]J. S. Rajachidambaram, S. Sanghavi, P. Nachimuthu, V. Shutthanandan, T. Varga, B. Flynn, S. Thevuthasan, and G. S. Herman, J. Mater. Res. **27**, 2309 (2012).
[55]R. Kelly and D. E. Harrison, Mater. Sci. Eng. **69**, 449 (1985).
[56]See http://www.npl.co.uk/science-technology/surface-and-nanoanalysis/services/sputter-yield-values for calculations of the sputtering yields of

Reuse of AIP Publishing content is subject to the terms at: https://publishing.aip.org/authors/rights-and-permissions. Download to IP: 131.111.184.102 On: Thu, 20 Oct 2016 10:33:10

elemental solids bombarded by ions such as Argon at various energies, using semi-empirical equation.
[57]D. F. Anthrop and A. W. Searcy, J. Phys. Chem. **68**, 2335 (1964).
[58]J. Kanicki and S. Martin, in *Thin-Film Transistors*, edited by C. R. Kagan and P. Andry (Marcel Dekker Inc., New York, 2003), p. 71.
[59]N. Mitoma, S. Aikawa, X. Gao, T. Kizu, M. Shimizu, M.-F. Lin, T. Nabatame, and K. Tsukagoshi, Appl. Phys. Lett. **104**, 102103 (2014).
[60]T. Kamiya and H. Hosono, NPG Asia Mater. **2**, 15 (2010).
[61]J. K. Jeong, J. H. Jeong, H. W. Yang, J.-S. Park, Y.-G. Mo, and H. D. Kim, Appl. Phys. Lett. **91**, 113505 (2007).
[62]J. Robertson, J. Non-Cryst. Solids **358**, 2437 (2012).
[63]K. M. Niang, J. Cho, A. Sadhanala, W. I. Milne, R. H. Friend, and A. J. Flewitt, "Zinc tin oxide thin film transistors produced by a high rate reactive sputtering: effect of tin composition and annealing temperatures," Phys. Status Solidi A (submitted).
[64]P. T. Erslev, E. S. Sundholm, R. E. Presley, D. Hong, J. F. Wager, and J. D. Cohen, Appl. Phys. Lett. **95**, 192115 (2009).

Reuse of AIP Publishing content is subject to the terms at: https://publishing.aip.org/authors/rights-and-permissions. Download to IP: 131.111.184.102 On: Thu, 20 Oct 2016 10:33:10